

# Revisiting the large extra dimension effects on $W$ -pair production at the LHC in NLO QCD

Bai Yu-Ming, Guo Lei, Li Xiao-Zhou, Ma Wen-Gan, and Zhang Ren-You  
Department of Modern Physics, University of Science and Technology  
of China (USTC), Hefei, Anhui 230026, People's Republic of China

## Abstract

In the framework of the large extra dimensions (LED) model, we investigate the effects induced by the Kaluza-Klein gravitons up to the QCD next-to-leading order (NLO) on the  $W$ -pair production followed by a subsequential  $W$ -decay at the CERN LHC. We depict the regions in the  $\mathcal{L} - M_S$  parameter space where the LED effect can and cannot be observed from the analyses of the  $pp \rightarrow W^+W^- + X$  and  $pp \rightarrow W^+W^- \rightarrow W^\pm l^\mp \bar{\nu} + X$  processes. We find that the ability of probing the LED effects can be improved by taking the cutoffs for the invariant mass of the  $W$ -pair and the transverse momentum of the final lepton. Our results demonstrate that the NLO QCD corrections to observables are significant, and do not show any improvement for the renormalization/factorization scale uncertainty on the QCD NLO corrected cross section, because the leading-order result underestimates the scale dependence.

PACS: 11.10.Kk, 12.38.Bx, 14.70.Fm

## I. Introduction

Motivated by the theoretical problems in the standard model (SM), many extended models beyond the SM have been established. Among them the large extra dimensions (LED) model proposed by Arkani-Hamed, Dimopoulos, and Dvali in Ref.[1] may be one of the promising models which can solve the long-standing mass hierarchy problem. This model used the idea of extra dimensions to bring gravity effects from the Plank scale down to the electroweak scale. In the LED model, the spacetime dimension is  $D = 4 + \delta$  with  $\delta$  being the dimension of extra space, where the gravity and gauge interactions are unified at one fundamental scale  $M_S \sim TeV$  (the order of the electroweak scale). The graviton propagates in the  $D$ -dimensional spacetime, while the SM particles exist only in the usual  $(3 + 1)$ -dimensions.

Taking into account of the bad behavior of quantum gravity in the ultraviolet (UV) region, it is expedient to construct a low-energy effective theory to describe the gravity-gauge-matter system in the current  $(3+1)$ -dimensional spacetime. In the phenomenological sense, this can be achieved through the Kaluza-Klein (KK) reduction in the brane-world scenario [2]. After applying this treatment to the LED model, a  $D$ -dimensional massless graviton can be perceived as a tower of massive KK modes propagating in the  $(3+1)$ -dimensional spacetime. It turns out that the weakness of gravitational coupling to the SM particles, suppressed by  $\overline{M}_P$  (the reduced Planck scale  $\overline{M}_P = \frac{M_P}{\sqrt{8\pi}}$ ), can be compensated by summing over numerous KK states. This scenario can result in distinct effects at the high-energy colliders [3]. Up to now, many studies on the virtual KK graviton effects up to the QCD next-to-leading order (NLO) in the LED model have emerged. These include the processes of fermion-pair, multijet, and vector-boson-pair production [4, 5, 6]. In Ref.[7] the CMS Collaboration has performed a search for LED in the diphoton final state events at the  $\sqrt{s} = 7 TeV$  LHC with an integrated luminosity of  $36 pb^{-1}$ . They set lower limits on the cutoff scale  $M_S$  in the range  $1.6 - 2.3 TeV$  at the 95% confidence level. The dijet angular distribution results from the CMS and ATLAS experiments appeared in Ref.[8] and provide even stronger limits on  $M_S$ , i.e.,  $M_S > 3.4 TeV$  (CMS) and  $M_S > 3.2 TeV$  (ATLAS). Recently, the production of a  $W$ -pair at hadronic colliders in the LED model has been studied up to the QCD NLO by Neelima Agarwal, *et al* [9].

In this paper, we revisit the NLO QCD corrections to the  $W$ -pair production process at the LHC in the framework of the LED model, and improve upon the results of Ref.[9] by including the effects of top-quark mass and the contribution from the  $b\bar{b}$ -fusion channel. We provide the LED effect discovery and exclusion regions, the kinematical distributions up to NLO in QCD by taking into account the subsequential  $W$ -boson leptonic decay. The rest of the paper is organized as follows. In Sec. II, we briefly go into the related Feynman rules in the LED model. In Sec. III, the leading-order(LO) cross section for the  $pp \rightarrow W^+W^- + X$  process is described. In Sec. IV, we calculate the NLO QCD corrections. In Sec. V, we present the numerical results for the LO and NLO QCD corrected integrated cross section for the  $W$ -pair production process and the distributions of final  $W$ -boson decay products. Finally, a short summary is given.

## II. Related theories

The LED model consists of the pure gravity sector and the SM sector. In this model the manifold, in which gravity propagates, is not the ordinary four-dimensional spacetime manifold  $\mathbb{R}^4$ , but  $\mathbb{R}^4 \times \mathcal{M}$ , where  $\mathcal{M}$  is a compact manifold of dimension  $\delta$ . For simplicity, one can tentatively assume that  $\mathcal{M}$  is a  $\delta$ -torus with radius  $R$  and volume  $V_\delta = (2\pi R)^\delta$  without loss of physical significance.

In our work we use the de Donder gauge. The Feynman rules for the propagator of the spin-2 KK graviton and the relevant vertices which we use are listed below. There  $G_{\text{KK}}^{\mu\nu}$ ,  $\psi$ ,  $W^{\pm\mu}$ ,  $A^{a\mu}$ , and  $\eta^a$  represent the fields of the graviton, quark,  $W$ -boson, gluon, and  $SU(3)$  ghost, respectively.

- spin-2 KK graviton propagator after summation over KK states :

$$\tilde{G}_{\text{KK}}^{\mu\nu\alpha\beta} = \frac{1}{2}D(s) \left[ \eta^{\mu\alpha}\eta^{\nu\beta} + \eta^{\mu\beta}\eta^{\nu\alpha} - \frac{2}{D-2}\eta^{\mu\nu}\eta^{\alpha\beta} \right] \quad (2.1)$$

- $G_{\text{KK}}^{\mu\nu}(k_3) - \bar{\psi}(k_1) - \psi(k_2)$  vertex :

$$-i\frac{1}{4\bar{M}_P} [\gamma^\mu(k_1+k_2)^\nu + \gamma^\nu(k_1+k_2)^\mu - 2\eta^{\mu\nu}(k_1+k_2 - 2m_\psi)] \quad (2.2)$$

- $G_{\text{KK}}^{\mu\nu}(k_4) - \bar{\psi}(k_1) - \psi(k_2) - A^{a\rho}(k_3)$  vertex :

$$ig_s\frac{1}{2\bar{M}_P} (\gamma^\mu\eta^{\nu\rho} + \gamma^\nu\eta^{\mu\rho} - 2\gamma^\rho\eta^{\mu\nu})T^a \quad (2.3)$$

- $G_{\text{KK}}^{\mu\nu}(k_3) - A^{a\rho}(k_1) - A^{b\sigma}(k_2)$  vertex :

$$i\frac{2}{\overline{M}_P}\delta^{ab}\left[(C^{\mu\nu\rho\sigma\tau\beta} - C^{\mu\nu\rho\beta\sigma\tau})k_{1\tau}k_{2\beta} + \frac{1}{\alpha_3}E^{\mu\nu\rho\sigma}(k_1, k_2)\right] \quad (2.4)$$

- $G_{\text{KK}}^{\mu\nu}(k_3) - W^{+\rho}(k_1) - W^{-\sigma}(k_2)$  vertex :

$$i\frac{2}{\overline{M}_P}\left[B^{\mu\nu\rho\sigma}m_W^2 + (C^{\mu\nu\rho\sigma\tau\beta} - C^{\mu\nu\rho\beta\sigma\tau})k_{1\tau}k_{2\beta} + \frac{1}{\xi}E^{\mu\nu\rho\sigma}(k_1, k_2)\right] \quad (2.5)$$

- $G_{\text{KK}}^{\mu\nu}(k_4) - A^{a\rho}(k_1) - A^{b\sigma}(k_2) - A^{c\lambda}(k_3)$  vertex :

$$\frac{2}{\overline{M}_P}g_s f^{abc}\left[(k_1 - k_3)_\tau C^{\mu\nu\tau\sigma\rho\lambda} + (k_2 - k_1)_\tau C^{\mu\nu\sigma\rho\tau\lambda} + (k_3 - k_2)_\tau C^{\mu\nu\lambda\sigma\tau\rho}\right] \quad (2.6)$$

- $G_{\text{KK}}^{\mu\nu}(k_5) - A^{a\rho}(k_1) - A^{b\sigma}(k_2) - A^{c\lambda}(k_3) - A^{d\delta}(k_4)$  vertex :

$$-i\frac{1}{\overline{M}_P}g_s^2[f^{eac}f^{ebd}D^{\mu\nu\rho\sigma\lambda\delta} + f^{eab}f^{ecd}D^{\mu\nu\rho\lambda\sigma\delta} + f^{ead}f^{ebc}D^{\mu\nu\rho\sigma\delta\lambda}] \quad (2.7)$$

- $G_{\text{KK}}^{\mu\nu}(k_3) - \bar{\eta}^a(k_1) - \eta^b(k_2)$  vertex :

$$-i\frac{2}{\overline{M}_P}\delta^{ab}B^{\alpha\beta\mu\nu}k_{1\alpha}k_{2\beta} \quad (2.8)$$

- $G_{\text{KK}}^{\mu\nu}(k_3) - \bar{\eta}^a(k_1) - \eta^b(k_2) - A^{c\rho}(k_3)$  vertex :

$$\frac{2}{\overline{M}_P}g_s f^{abc}B^{\alpha\rho\mu\nu}k_{1\alpha} \quad (2.9)$$

where  $g_s$  is the strong coupling constant,  $T^a$  and  $f^{abc}$  are SU(3) generators and structure constants,  $D = n + \delta$ ,  $n = 4 - 2\epsilon$ ,  $\overline{M}_p$  is the reduced Planck mass,  $\alpha_3$  and  $\xi$  are SU(3) and charged SU(2) gauge fixing parameters, and  $D(s)$  can be expressed as [2]

$$D(s) = \frac{s^{\delta/2-1} R^\delta}{\Gamma(\delta/2) (4\pi)^{\delta/2}} \left[ \pi + 2iI(\Lambda/\sqrt{s}) \right] \quad (2.10)$$

and

$$I(\Lambda/\sqrt{s}) = P \int_0^{\Lambda/\sqrt{s}} dy \frac{y^{\delta-1}}{1-y^2} . \quad (2.11)$$

The integral  $I(\Lambda/\sqrt{s})$  contains an ultraviolet cutoff  $\Lambda$  on the KK modes [2, 3]. In this work we set it to be the fundamental scale  $M_S$ . It should be understood that a point  $y = 1$  has been removed from the integration path. Besides, all the momenta are assumed to be incoming to

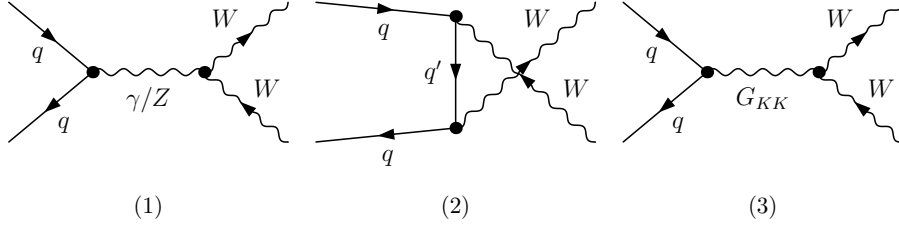


Figure 1: The tree-level Feynman diagrams for the partonic processes  $q\bar{q} \rightarrow W^+W^-$  in the LED model. (1) and (2) are the SM-like diagrams, where  $q$  represents the  $u$ -,  $d$ -,  $c$ -,  $s$ - and  $b$ -quark. (3) is the extra diagram with KK graviton exchange.

the vertices, except that the fermionic momenta are set to be along the fermion flow directions.

The coefficients  $A^{\mu\nu}$ ,  $B^{\mu\nu\alpha\beta}$ ,  $C^{\rho\sigma\mu\alpha\beta}$ ,  $D^{\mu\nu\rho\sigma\lambda\delta}$ , and  $E^{\mu\nu\rho\sigma}(k_1, k_2)$  are expressed as

$$\begin{aligned}
A^{\mu\nu} &= \frac{1}{2}\eta^{\mu\nu}, & B^{\mu\nu\alpha\beta} &= \frac{1}{2}(\eta^{\mu\nu}\eta^{\alpha\beta} - \eta^{\mu\alpha}\eta^{\nu\beta} - \eta^{\mu\beta}\eta^{\nu\alpha}), \\
C^{\rho\sigma\mu\alpha\beta} &= \frac{1}{2}[\eta^{\rho\sigma}\eta^{\mu\nu}\eta^{\alpha\beta} - (\eta^{\rho\mu}\eta^{\sigma\nu}\eta^{\alpha\beta} + \eta^{\rho\nu}\eta^{\sigma\mu}\eta^{\alpha\beta} + \eta^{\rho\alpha}\eta^{\sigma\beta}\eta^{\mu\nu} + \eta^{\rho\beta}\eta^{\sigma\alpha}\eta^{\mu\nu})], \\
D^{\mu\nu\rho\sigma\lambda\delta} &= \eta^{\mu\nu}(\eta^{\rho\sigma}\eta^{\lambda\delta} - \eta^{\rho\delta}\eta^{\sigma\lambda}) + (\eta^{\mu\rho}\eta^{\nu\delta}\eta^{\lambda\sigma} + \eta^{\mu\lambda}\eta^{\nu\sigma}\eta^{\rho\delta} - \eta^{\mu\rho}\eta^{\nu\sigma}\eta^{\lambda\delta} - \eta^{\mu\lambda}\eta^{\nu\delta}\eta^{\rho\sigma} + (\mu \leftrightarrow \nu)), \\
E^{\mu\nu\rho\sigma}(k_1, k_2) &= \eta^{\mu\nu}(k_1^\rho k_1^\sigma + k_2^\rho k_2^\sigma + k_1^\rho k_2^\sigma) - [\eta^{\nu\sigma}k_1^\mu k_1^\rho + \eta^{\nu\rho}k_2^\mu k_2^\sigma + (\mu \leftrightarrow \nu)].
\end{aligned}$$

We code programmatically the related Feynman rules in the FeynArts 3.5 package [10] to generate the Feynman diagrams and the relevant amplitudes. The FormCalc 5.4 [11] package is implemented subsequently to simplify the amplitudes.

### III. LO cross section for $pp \rightarrow W^+W^- + X$

We treat the up-, down-, charm-, strange-, and bottom-quark as massless particles, and adopt the five-flavor scheme in the leading order and QCD next-to-leading order calculations. The LO contribution to the parent process  $pp \rightarrow W^+W^- + X$  includes the quark-antiquark ( $q = u, d, s, c, b$ ) annihilations and the gluon-gluon fusion partonic processes:  $q(p_1) + \bar{q}(p_2) \rightarrow W^+(p_3) + W^-(p_4)$  and  $g(p_1) + g(p_2) \rightarrow W^+(p_3) + W^-(p_4)$ . There  $p_i$  ( $i = 1, 2, 3, 4$ ) represent the four-momenta of the incoming and outgoing particles, respectively. The corresponding Feynman diagrams are shown in Figs.1 and 2. Figures.1(1) and .1(2) are the LO SM-like diagrams for partonic process  $q\bar{q} \rightarrow W^+W^-$ . In Fig.1(1) the internal wavy line means exchanging  $\gamma$  or a  $Z^0$ -boson. There we ignore the diagrams with exchanging Higgs boson, since the initial quarks are all massless.

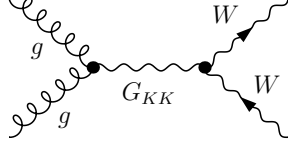


Figure 2: The tree-level Feynman diagram for the partonic process  $gg \rightarrow W^+W^-$  in the LED model.

We express the tree-level amplitudes for the partonic processes  $q\bar{q} \rightarrow W^+W^-$  and  $gg \rightarrow W^+W^-$  as

$$\mathcal{M}_{q\bar{q}}^0 = \mathcal{M}_{q\bar{q}}^{0,SM} + \mathcal{M}_{q\bar{q}}^{0,LED}, \quad \mathcal{M}_{gg}^0 = \mathcal{M}_{gg}^{0,LED}, \quad (3.1)$$

where  $\mathcal{M}_{q\bar{q}}^{0,SM}$  ( $q = u, d, c, s, b$ ) is the amplitude contributed by the tree-level SM-like diagrams, while  $\mathcal{M}_{q\bar{q}}^{0,LED}$  and  $\mathcal{M}_{gg}^{0,LED}$  are the tree-level amplitudes with KK graviton exchange. Our calculations show that the analytical expression of the SM matrix element squares summed (averaged) over the final (initial) state spins and colors at the LO,  $|\overline{\mathcal{M}_{q\bar{q}}^{0,SM}}|^2$ , for the partonic process without massive internal or external quark (i.e.,  $q = u, d, c, s$ ), is the same as that presented in Ref.[9]. But for the partonic process  $b\bar{b} \rightarrow W^+W^-$ , there is a t-channel diagram with a massive top-quark exchange. Its explicit expression of  $|\overline{\mathcal{M}_{b\bar{b}}^{0,SM}}|^2$  is presented below by adopting the notations in Ref.[9].

$$|\overline{\mathcal{M}_{b\bar{b}}^{0,SM}}|^2 = \frac{e^4}{N} \left( A_1^b B_{1m}^b + A_2^b B_{2m}^b + A_3^b B_{3m}^b \right), \quad (3.2)$$

where  $N$  is the number of colors. The explicit expressions for  $A_1^b$ ,  $A_2^b$ , and  $A_3^b$  can be obtained from the Eqs.(8) in Ref.[9] by taking the replacement of  $u \rightarrow b$ . The kinematic invariants  $B_{1m}^b$ ,  $B_{2m}^b$ , and  $B_{3m}^b$  can be expressed as

$$B_{1m}^b = \frac{u^2}{(u - m_t^2)^2} B_1^d(t, u, s), \quad B_{2m}^b = B_2^d(t, u, s), \quad B_{3m}^b = \frac{u}{(u - m_t^2)} B_3^d(t, u, s), \quad (3.3)$$

where  $B_1^d(t, u, s)$ ,  $B_2^d(t, u, s)$  and  $B_3^d(t, u, s)$  are presented in Eqs.(9)-(12) of Ref.[9]. Then the LO cross sections for the unpolarized  $W$ -pair production processes at the partonic level can be expressed as

$$\hat{\sigma}_{ij}^{LO} = \frac{1}{4|\vec{p}|\sqrt{\hat{s}}} \int d\Gamma_2 |\overline{\mathcal{M}_{ij}^0}|^2, \quad (ij = u\bar{u}, d\bar{d}, c\bar{c}, s\bar{s}, b\bar{b}, gg), \quad (3.4)$$

where  $\vec{p}$  is the momentum of one initial parton in center-of-mass system (c.m.s.) and  $d\Gamma_2$  is the two-body phase space element expressed as

$$d\Gamma_2 = (2\pi)^4 \delta^{(4)}(p_1 + p_2 - p_3 - p_4) \prod_{i=3,4} \frac{d^3\vec{p}_i}{(2\pi)^3 2E_i}. \quad (3.5)$$

By convoluting  $\hat{\sigma}_{ij}^{LO}$  with the parton distribution functions (PDFs) of the colliding protons, the LO cross section for the parent process,  $pp \rightarrow W^+W^- + X$ , can be written as

$$\sigma_{LO} = \sum_{ij=u\bar{u}, d\bar{d}, s\bar{s}}^{c\bar{c}, b\bar{b}, gg} \frac{1}{1 + \delta_{ij}} \int dx_A dx_B \left[ G_{i/A}(x_A, \mu_f) G_{j/B}(x_B, \mu_f) \hat{\sigma}_{ij}^{LO}(\sqrt{\hat{s}}) + (i \leftrightarrow j) \right], \quad (3.6)$$

where  $G_{i/P}$  ( $i = g, q, \bar{q}$ ) represent the PDFs of parton  $i$  in proton  $P$ ,  $\mu_f$  is the factorization scale,  $\sqrt{\hat{s}} = x_A x_B \sqrt{s}$ ,  $x_A$  and  $x_B$  describe the momentum fractions of parton (gluon or quark) in protons  $A$  and  $B$ , respectively.

## IV. NLO QCD corrections

The complete NLO QCD correction to the parent process  $pp \rightarrow W^+W^- + X$  consists of following components. (1) The virtual contribution from the QCD one-loop and the corresponding counterterm diagrams to the partonic channels  $q\bar{q} \rightarrow W^+W^-$  and  $gg \rightarrow W^+W^-$ . (2) The contribution of the real gluon emission partonic processes. (3) The contribution of the real light-(anti)quark emission partonic processes. And (4) the corresponding contribution of the PDF counterterms. There inevitably exist the ultraviolet (UV) and infrared (IR) divergences in the NLO calculations, and we adopt the dimensional regularization scheme in  $n = 4 - 2\epsilon$  dimensions to isolate and manipulate these divergences.

### A. Virtual corrections

The Feynman diagrams for the virtual corrections to the  $q\bar{q} \rightarrow W^+W^-$  and  $gg \rightarrow W^+W^-$  partonic processes are shown in Fig.3 and Fig.4, respectively. In Figs.4(3) and .4(4) the diagrams involving Yukawa coupling between Higgs boson and top quarks are included, but the diagrams involving Yukawa coupling between Higgs boson and massless quarks are excluded due to their vanishing contribution. There exist UV and soft/collinear IR singularities in the calculations of these one-loop diagrams. To remove the UV divergences, we need only the wave function

renormalization constants for the quark and gluon fields. We introduce the renormalization constants  $\delta Z_{\psi_{q,L,R}}$  for massless quark ( $q=u,d,c,s,b$ ) fields and  $\delta Z_A$  for the gluon field defined as

$$\psi_{q,L,R}^0 = (1 + \delta Z_{\psi_{q,L,R}})^{1/2} \psi_{q,L,R}, \quad A_\mu^{a0} = (1 + \delta Z_A)^{1/2} A_\mu^a. \quad (4.1)$$

In the modified minimal subtraction ( $\overline{MS}$ ) renormalization scheme the renormalization constants for the massless quarks are expressed as

$$\delta Z_{\psi_{q,L}} = -\frac{\alpha_s}{4\pi} C_F (\Delta_{UV} - \Delta_{IR}), \quad \delta Z_{\psi_{q,R}} = -\frac{\alpha_s}{4\pi} C_F (\Delta_{UV} - \Delta_{IR}), \quad (4.2)$$

$$\delta Z_A = \frac{\alpha_s}{4\pi} \left( \frac{5}{3} C_A - \frac{4}{3} n_f^{UV} T_F \right) \Delta_{UV} + \frac{\alpha_s}{4\pi} \left( \frac{5}{3} C_A - \frac{4}{3} n_f^{IR} T_F \right) \Delta_{IR}, \quad (4.3)$$

To remove the UV and IR divergences in the  $b\bar{b}$ -fusion subprocess, we need introduce the counterterms for the top-quark field and its mass, i.e.,

$$\psi_{t,L,R}^0 = (1 + \delta Z_{\psi_{t,L,R}})^{1/2} \psi_{t,L,R}, \quad m_t^0 = m_t + \delta m_t. \quad (4.4)$$

We use the on-mass-shell scheme to renormalize the top-quark field and mass. They are expressed as

$$\delta Z_{\psi_{t,L}} = -\frac{\alpha_s}{4\pi} C_F (\Delta_{UV} + 2\Delta_{IR} + 3 \ln \frac{\mu_r^2}{m_t^2} + 4), \quad (4.5)$$

$$\delta Z_{\psi_{t,R}} = -\frac{\alpha_s}{4\pi} C_F (\Delta_{UV} + 2\Delta_{IR} + 3 \ln \frac{\mu_r^2}{m_t^2} + 4), \quad (4.6)$$

$$\frac{\delta m_t}{m_t} = -\frac{3\alpha_s}{4\pi} C_F (\Delta_{UV} + \ln \frac{\mu_r^2}{m_t^2} + \frac{4}{3}), \quad (4.7)$$

In the above equations  $\mu_r$  is the renormalization scale,  $C_F = \frac{4}{3}$ ,  $C_A = 3$ ,  $T_F = \frac{1}{2}$ ,  $n_f^{UV} = 6$  corresponds to the six flavor quarks ( $u, d, c, s, t, b$ ), whereas  $n_f^{IR} = 5$  is the number of the massless quarks ( $u, d, s, c, b$ ). Moreover,  $\Delta_{UV} = \frac{1}{\epsilon_{UV}} \Gamma(1 + \epsilon_{UV}) (4\pi)^{\epsilon_{UV}}$  and  $\Delta_{IR} = \frac{1}{\epsilon_{IR}} \Gamma(1 + \epsilon_{IR}) (4\pi)^{\epsilon_{IR}}$  refer to the UV and IR divergences, respectively.

Then the results for the differential cross sections for the  $q\bar{q}$  annihilation and  $gg$  fusion partonic channels are UV finite but soft/collinear IR divergent. The soft/collinear IR singularities can be canceled by adding the contributions of the real emission partonic processes and the corresponding PDF counterterms.

## B. Real gluon emission



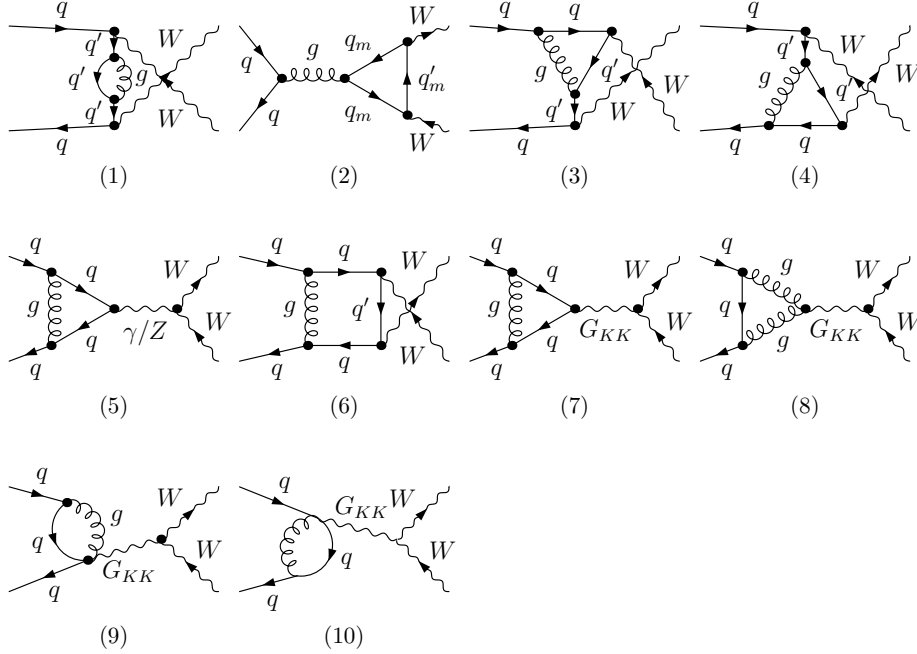


Figure 3: The QCD one-loop Feynman diagrams for the partonic process  $q\bar{q} \rightarrow W^+W^-$ . (1)-(6) are the SM-like diagrams. (7)-(10) are the diagrams with KK graviton exchange.

The real gluon emission contributions are from  $g(p_1) + g(p_2) \rightarrow W^+(p_3) + W^-(p_4) + g(p_5)$  and  $q(p_1) + \bar{q}(p_2) \rightarrow W^+(p_3) + W^-(p_4) + g(p_5)$  partonic processes. The corresponding Feynman diagrams are shown in Fig.5 and Fig.6, respectively. We employ the two cutoff phase space slicing (TCPSS) method [12] to calculate the contributions from the real gluon emission partonic processes. An arbitrary soft cutoff  $\delta_s$  is introduced to separate the gluon emission subprocess phase space into two regions, soft gluon and hard gluon regions. Furthermore, another cutoff  $\delta_c$  is introduced to decompose the real hard gluon emission phase space region into hard collinear ( $HC$ ) and hard noncollinear ( $\overline{HC}$ ) regions. The partonic differential cross section for the real gluon emission subprocess can be expressed as

$$d\hat{\sigma}_g = d\hat{\sigma}_g^S + d\hat{\sigma}_g^H = d\hat{\sigma}_g^S + d\hat{\sigma}_g^{HC} + d\hat{\sigma}_g^{\overline{HC}}. \quad (4.8)$$

### C. Real light-(anti)quark emission

In addition to the real gluon emission discussed above, there are contributions from the massless light-(anti)quark ( $u, d, c, s, b, \bar{u}, \bar{d}, \bar{c}, \bar{s}, \bar{b}$ ) emission partonic processes. In the five-flavor scheme the massless light-quark  $q$  involves  $u$ -,  $d$ -,  $c$ -,  $s$ -,  $b$ -quarks. Considering the fact that

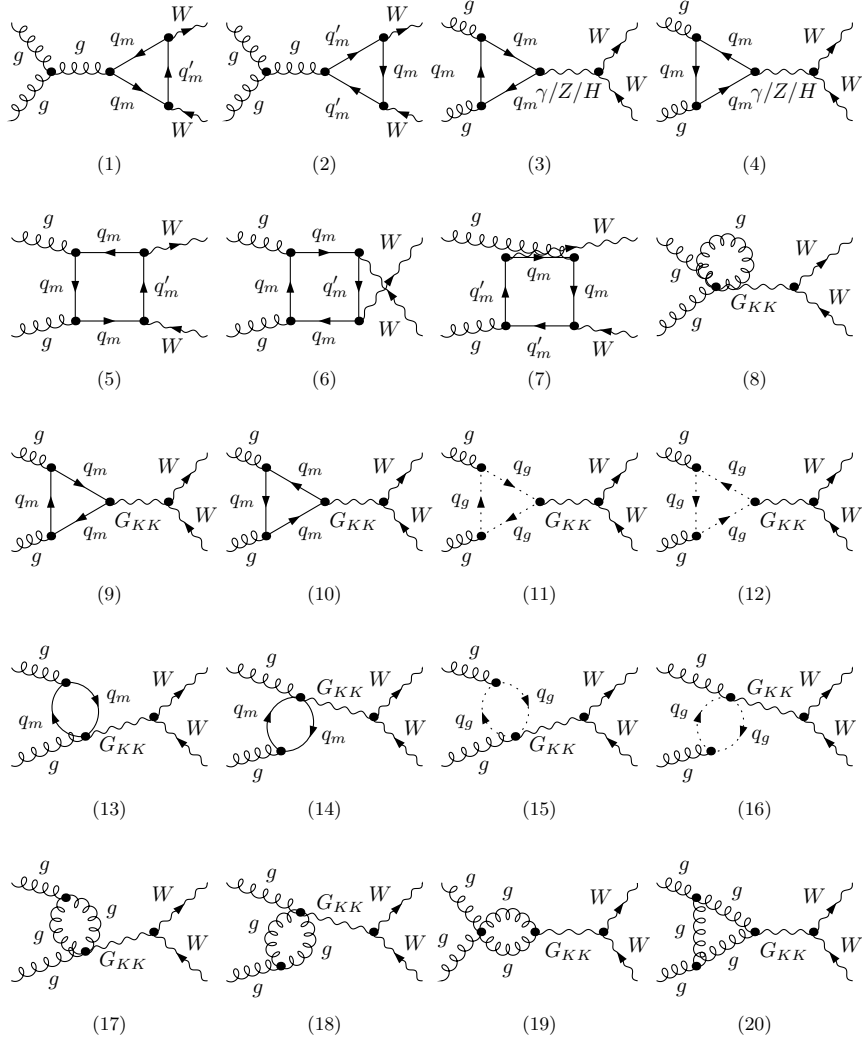


Figure 4: The QCD one-loop Feynman diagrams for partonic process  $gg \rightarrow W^+W^-$ . (1)-(7) are the SM-like diagrams. (8)-(20) are the diagrams with KK graviton exchange. In all diagrams  $q_m$  represents  $u$ -,  $d$ -,  $c$ -,  $s$ -,  $b$ - and  $t$ -quark except the diagrams in Figs.4(3) and Fig.4(4) involving the coupling between Higgs boson and top quarks, where  $q_m$  denotes only top quark.

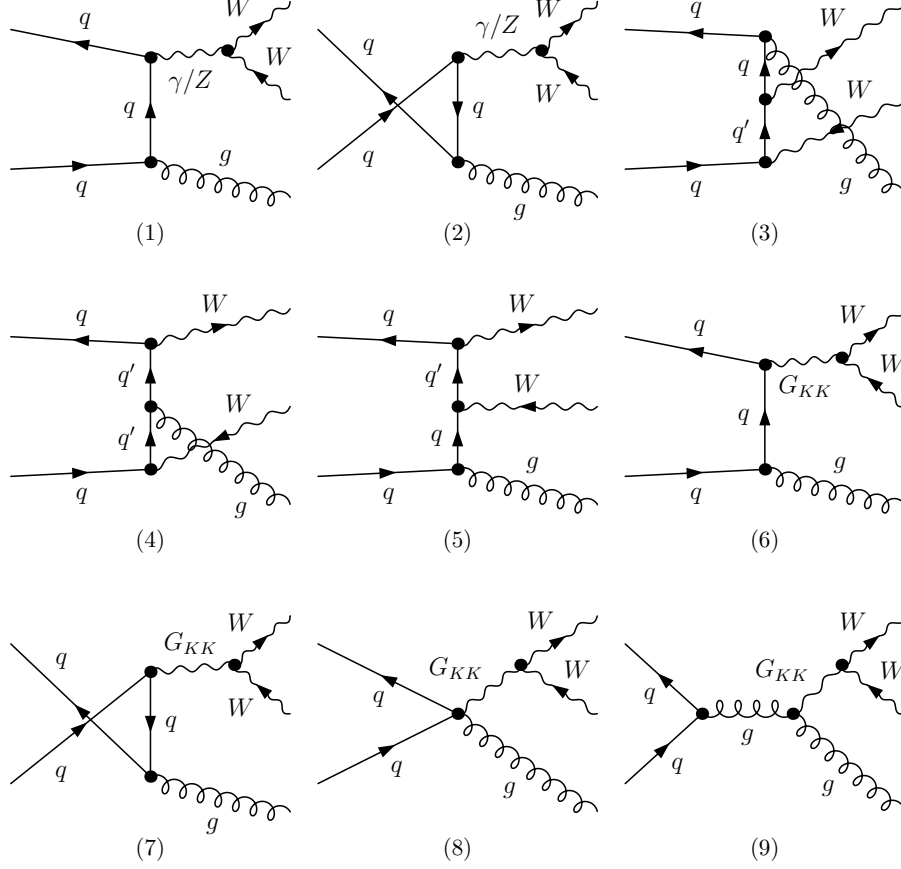


Figure 5: The tree-level Feynman diagrams for the real gluon emission subprocess  $q\bar{q} \rightarrow W^+W^-g$ . (1)-(5) are the SM-like diagrams. (6)-(9) are the extra diagrams with KK graviton exchange.

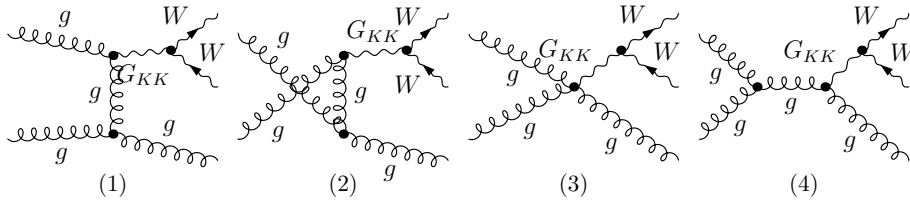


Figure 6: The tree-level Feynman diagrams for the real gluon emission subprocess  $gg \rightarrow W^+W^-g$ . There is no SM-like diagram.

the final (anti)bottom-quark can be tagged in experiments and the collinear IR singularities of the real (anti)bottom-quark emission subprocesses are completely canceled by those of the corresponding PDF counter terms, we do not include the contributions of the bottom and antibottom emissions, and adopt the five-flavor PDFs [13]. We depict the Feynman diagrams for the partonic processes  $qg \rightarrow W^+W^- + q$  and  $\bar{q}g \rightarrow W^+W^- + \bar{q}$  in Fig.7. These partonic processes contain only the initial state collinear singularities. By using the TCPSS method described above, we can split the phase space into collinear and noncollinear regions. The differential cross sections for the partonic processes  $qg \rightarrow W^+W^-q$  and  $\bar{q}g \rightarrow W^+W^-\bar{q}$  can then be expressed as

$$d\hat{\sigma}_{q(\bar{q})}(q(\bar{q})g \rightarrow W^+W^-q(\bar{q})) = d\hat{\sigma}_{q(\bar{q})}^C + d\hat{\sigma}_{q(\bar{q})}^{\bar{C}}, \quad (4.9)$$

where  $d\hat{\sigma}_q^{\bar{C}}$  and  $d\hat{\sigma}_{\bar{q}}^{\bar{C}}$  are finite and can be evaluated by using the general Monte Carlo method.

#### D. NLO QCD corrections to the $pp \rightarrow W^+W^- + X$ process

Combining the renormalized virtual corrections and the real gluon/light-(anti)quark emission contributions, the partonic cross sections still contain the collinear divergence, which can be absorbed into the redefinition of the PDFs at the NLO according to the mass factorization [14]. We find that after the summation of all the NLO QCD corrections, the soft and collinear IR divergences vanish. We can see from above discussion that the final total  $\mathcal{O}(\alpha_s)$  corrections consist of the two-body term  $\sigma^{(2)}$  and the three-body term  $\sigma^{(3)}$ . The total cross section up to the QCD NLO is expressed as

$$\sigma_{NLO} = \sigma_{LO} + \Delta\sigma_{NLO} = \sigma_{LO} + \sigma^{(2)} + \sigma^{(3)}. \quad (4.10)$$

It is UV finite, IR safe, and cutoff  $\delta_c/\delta_s$  independent [12, 15], which will further be checked in the numerical evaluations.

## V. Numerical results and discussions

In this section, we present the numerical results of the integrated cross sections and the kinematic distributions of the final particles for the  $pp \rightarrow W^+W^- + X$  process in both the SM and LED

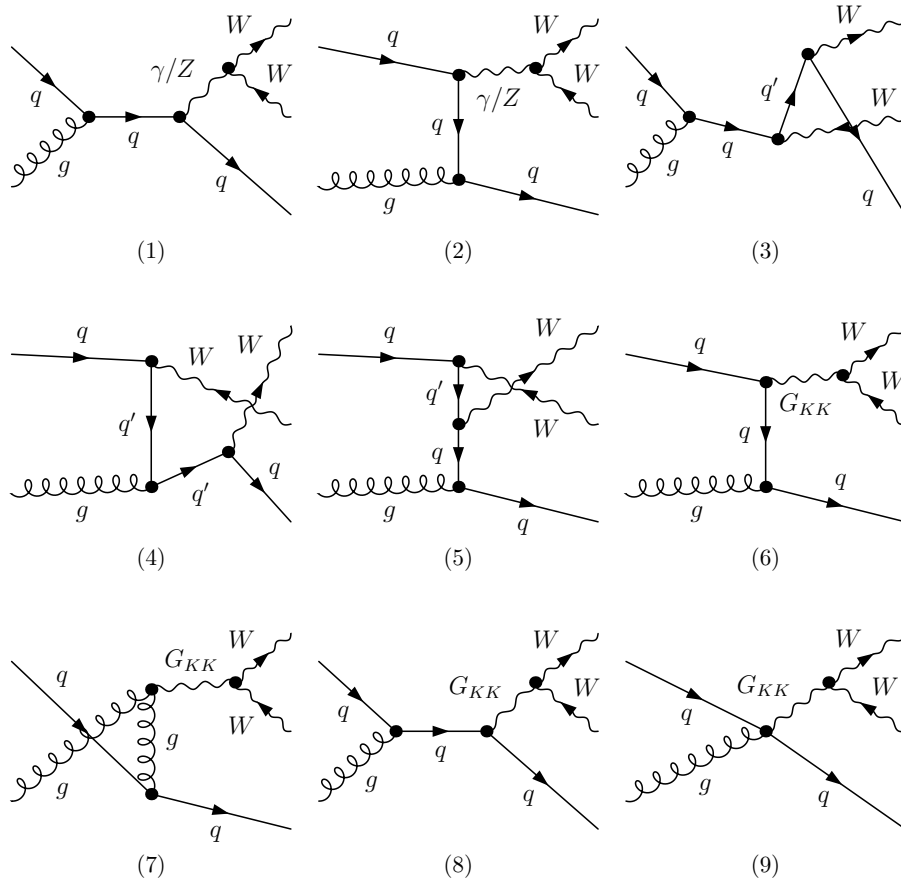


Figure 7: The tree-level Feynman diagrams for the real light-(anti)quark emission subprocesses  $q(\bar{q})g \rightarrow W^+W^-q(\bar{q})$ . (1)-(5) are the SM-like diagrams. (6)-(9) are the diagrams with KK graviton exchange.

model up to the QCD NLO. In order to verify the correctness of our numerical calculations, we made the following checks:

- (i) In Table 1, we list our numerical results of the LO and NLO QCD corrected integrated cross sections in the SM for the  $pp \rightarrow W^+W^- + X$  process by taking the input parameters, PDFs, and event selection criterion from Table 4 of Ref.[16]. It shows that our LO and NLO QCD corrected cross sections in the SM are in good agreement with those in Ref.[16] within the integration errors.

LHC	Ref.[16]	FeynArts	CompHEP
Born[pb]	86.7	86.711(6)	86.7(1)
NLO QCD[pb]	127.8	127.7(1)	—

Table 1: The LO and NLO QCD corrected cross sections for the  $pp \rightarrow W^+W^- + X$  process in the SM by taking the same input parameters and event selection criterion as those in Ref.[16].

- (ii) The UV and IR safeties are verified numerically after combining all the contributions at the QCD NLO.
- (iii) We calculate the NLO QCD corrections to integrated cross section for the  $pp \rightarrow u\bar{u} \rightarrow W^+W^- + X$  process as functions of the cutoff  $\delta_s$  at the  $\sqrt{s} = 14 \text{ TeV}$  LHC in the LED model, where we take  $\mu_f = \mu_r = \mu_0 = m_W$ ,  $M_S = 3.5 \text{ TeV}$ ,  $\delta = 3$  and  $\delta_c = \delta_s/50$ . Some of the results are listed in Table 2. It is shown clearly that the NLO QCD correction ( $\Delta\sigma_{NLO}^{LED}$ ) does not depend on the arbitrarily chosen values of  $\delta_s$  and  $\delta_c$  within the calculation errors. In the further numerical calculations, we fix  $\delta_s = 10^{-3}$  and  $\delta_c = \delta_s/50$ .
- (iv) We calculate the SM LO  $W$ -pair invariant mass distribution ( $d\sigma_{LO}^{SM}/dM_{WW}$ ) for the  $pp \rightarrow W^+W^- + X$  process with the same input parameters, PDFs and event selection criterion as those used in Ref.[9]. The numerical results, which are obtained by using FeynArts and CompHEP packages separately, are coincident with each other.
- (v) For further comparison with the previous work of N. Agarwal, *et al*, we recalculate the LO and NLO QCD corrected distributions of  $W$ -pair invariant mass in both the SM and LED model ( $d\sigma_{LO}^{SM,LED}/dM_{WW}$ ,  $d\sigma_{NLO}^{SM,LED}/dM_{WW}$ ) for the  $pp \rightarrow W^+W^- + X$  process at the

$\delta_s$	$\Delta\sigma_{NLO}^{LED}[\text{pb}]$
$2 \times 10^{-3}$	13.19(3)
$1 \times 10^{-3}$	13.20(3)
$7 \times 10^{-4}$	13.21(3)
$4 \times 10^{-4}$	13.22(5)
$2 \times 10^{-4}$	13.24(5)
$1 \times 10^{-4}$	13.26(6)
$7 \times 10^{-5}$	13.25(6)
$4 \times 10^{-5}$	13.27(6)
$2 \times 10^{-5}$	13.26(7)

Table 2: The dependence of the NLO QCD correction to the integrated cross section for the process  $pp \rightarrow u\bar{u} \rightarrow W^+W^- + X$  at the  $\sqrt{s} = 14 \text{ TeV}$  LHC in the LED model, where we set  $\mu_f = \mu_r = \mu_0 = m_W$ ,  $M_S = 3.5 \text{ TeV}$ ,  $\delta = 3$  and  $\delta_c = \delta_s/50$ .

$\sqrt{s} = 14 \text{ TeV}$  LHC, where we set all the quarks being massless except  $m_t = 172.0 \text{ GeV}$ , and take the PDFs and event selection criterion from Ref.[9]. We plot our LO and NLO QCD corrected results in the SM in Fig.8(a), and the results in the LED model in Fig.8(b). In these two figures we depict also the corresponding curves from N. Agarwal's paper [9] for comparison. We can see that there exist obvious discrepancies between ours and the corresponding N. Agarwal results, especially in the large  $M_{WW}$  region. One of the reasons for the disagreement is because we have included the effects of top-quark mass in our calculations. From Figs.8(a,b) we can see the K-factors of the QCD corrections increase to large numbers of  $K = 5.29$  and  $K = 2.33$  separately, when  $W$ -pair invariant mass approaches  $M_{WW} = 1300 \text{ GeV}$ . This occurs because the K-factors in Figs.8(a,b) are the results with only constraint on  $W$ -bosons ( $|y_W| < 2.5$ ) [9]. In this case the differential cross section,  $d\sigma_{NLO}^{SM}/dM_{WW}$ , receives a large contribution from the hard jet emission corrections ( $W^+W^- + jet$ ). For example, in Fig.8(a) at  $M_{WW} = 1300 \text{ GeV}$  the K-factor contributed by hard jet emission processes can reach 3.59.

In the following calculations we take one-loop and two-loop running  $\alpha_s$  in the LO and QCD NLO calculations, respectively [17]. The QCD parameters are taken as  $\Lambda_5^{LO} = 165 \text{ MeV}$ ,  $\Lambda_5^{\overline{MS}} = 226 \text{ MeV}$ , the number of the active flavors is  $n_f = 5$ , the Cabibbo-Kobayashi-Maskawa matrix is set as a unit matrix, and the colliding c.m.s. energy is taken as  $\sqrt{s} = 7 \text{ TeV}$  and  $\sqrt{s} = 14 \text{ TeV}$  for the early and future LHC. To satisfy the unitary constraint, we adopt the

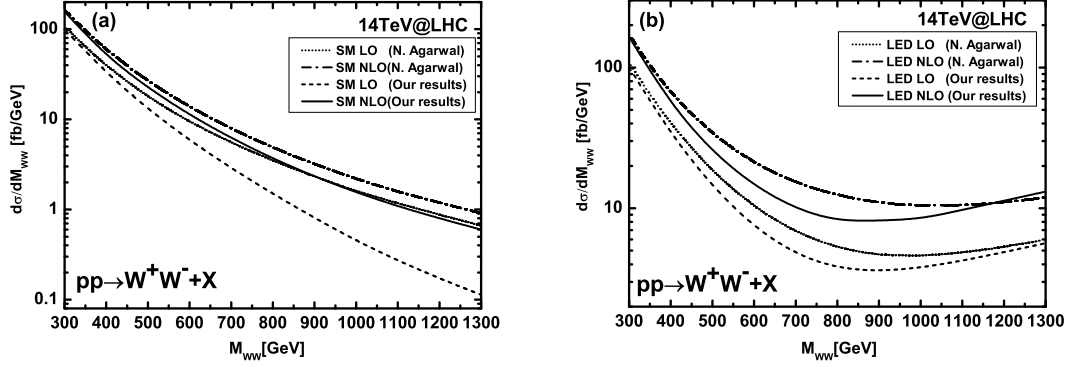


Figure 8: Invariant mass ( $M_{WW}$ ) distributions at the LO and NLO for the  $pp \rightarrow W^+W^- + X$  process at the  $\sqrt{s} = 14 \text{ TeV}$  LHC. There the input parameters, PDFs, and event selection criterion are taken from Ref.[9] (where  $M_S = 2 \text{ TeV}$ ,  $\delta = 3$ , and  $\mu_r = \mu_f = M_{WW}$ ). For comparison with previous work, we depict also the corresponding curves from N. Agarwal's paper [9] in both panels. (a) The distributions in the SM. (b) The distributions in the LED model.

cut  $\sqrt{\hat{s}} < M_S$  for the whole phase space. We assume  $m_H = 120 \text{ GeV}$  and the renormalization and factorization scales to be equal ( $\mu_r = \mu_f \equiv \mu$ ), and we define  $\mu_0 \equiv m_W$ . We use the CTEQ6L1 and CTEQ6M PDFs [18, 19] in the LO and QCD NLO calculations, respectively. The other related input parameters are taken from [17]:  $\alpha^{-1}(m_Z) = 127.916$ ,  $m_W = 80.399 \text{ GeV}$ ,  $m_Z = 91.1876 \text{ GeV}$  and  $m_t = 172.0 \text{ GeV}$ . As we know that the constraints on the final particles are necessary in realistic experimental event collections, and the theoretical calculation should keep the perturbative convergence. We adopt the following event selection constraints additionally. (1) For the real emission contributions, we accept the events which satisfy the condition that the jet pseudorapidity  $|y_{jet}| > 2.5$  or the jet transverse momentum  $p_T^{jet} < 50 \text{ GeV}$ . (2) The  $W$ -pair invariant mass is restricted in the range of  $M_{WW} > 400 \text{ GeV}$ .

In Figs.9(a,b), the upper panels show the scale ( $\mu$ ) dependence of the LO and the NLO QCD corrected cross sections in the SM and LED model at the  $\sqrt{s} = 7 \text{ GeV}$  and  $\sqrt{s} = 14 \text{ TeV}$  LHC separately, and the corresponding  $K$ -factors ( $K(\mu) \equiv \frac{\sigma_{NLO}(\mu)}{\sigma_{LO}(\mu)}$ ) are illustrated in the lower panels. There we take  $M_S = 3.5 \text{ TeV}$  and  $\delta = 3$ . The scale-dependent  $K$ -factor in the LED model varies from 1.18 (1.53) to 1.19 (1.11) when  $\mu$  goes from  $0.5\mu_0$  to  $2\mu_0$  at the  $\sqrt{s} = 7 \text{ TeV}$  LHC (the  $\sqrt{s} = 14 \text{ TeV}$  LHC). We see from these upper panels that the NLO QCD corrections



in the SM and LED model do not reduce the factorization/renormalization scale uncertainty, especially at the  $\sqrt{s} = 14 \text{ TeV}$  LHC. That is because the LO result underestimates the scale dependence due to the LO contribution being from pure electroweak partonic processes. And we find that the  $K$ -factors plotted in the lower figures keep the convergence of the perturbative series in the plotted  $\mu$  range at both the  $\sqrt{s} = 7 \text{ TeV}$  and  $\sqrt{s} = 14 \text{ TeV}$  LHC. In further calculations we fix  $\mu = m_W$ .

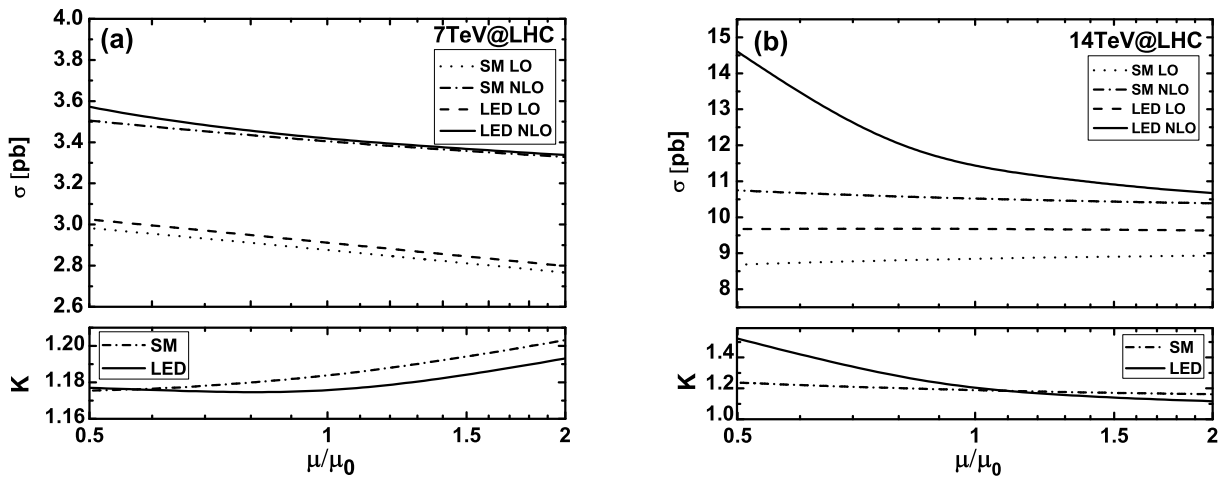


Figure 9: The scale dependence of the LO and NLO QCD corrected cross sections for the process  $pp \rightarrow W^+W^- + X$  in the SM and LED model, and the corresponding  $K$ -factor [ $K(\mu) \equiv \frac{\sigma_{NLO}(\mu)}{\sigma_{LO}(\mu)}$ ] with  $M_S = 3.5 \text{ TeV}$  and  $\delta = 3$ . (a) At the  $\sqrt{s} = 7 \text{ TeV}$  LHC. (b) At the  $\sqrt{s} = 14 \text{ TeV}$  LHC.

In Figs.10(a,b), we depict the LO and NLO QCD corrected cross sections and the corresponding  $K$ -factors for the process  $pp \rightarrow W^+W^- + X$  in the LED model as the functions of the fundamental scale  $M_S$ , with  $\mu = m_W$  and the extra space dimension number  $\delta$  being 3, 4, and 5, respectively. From the figures one can find that the more distinct LED effect exhibits with the smaller values of  $M_S$  and  $\delta$ .

The LO and NLO QCD corrected distributions of the  $W$ -pair invariant mass and the corresponding  $K$ -factors ( $K(M_{WW}) \equiv \frac{d\sigma_{NLO}}{dM_{WW}} / \frac{d\sigma_{LO}}{dM_{WW}}$ ) for the process  $pp \rightarrow W^+W^- + X$  in the SM and LED model at the early and future LHC, are shown in Figs.11(a) and (b), separately. There the results are for  $M_S = 3.5 \text{ TeV}$ ,  $\mu = m_W$ , at a fixed value 3 for the number of extra

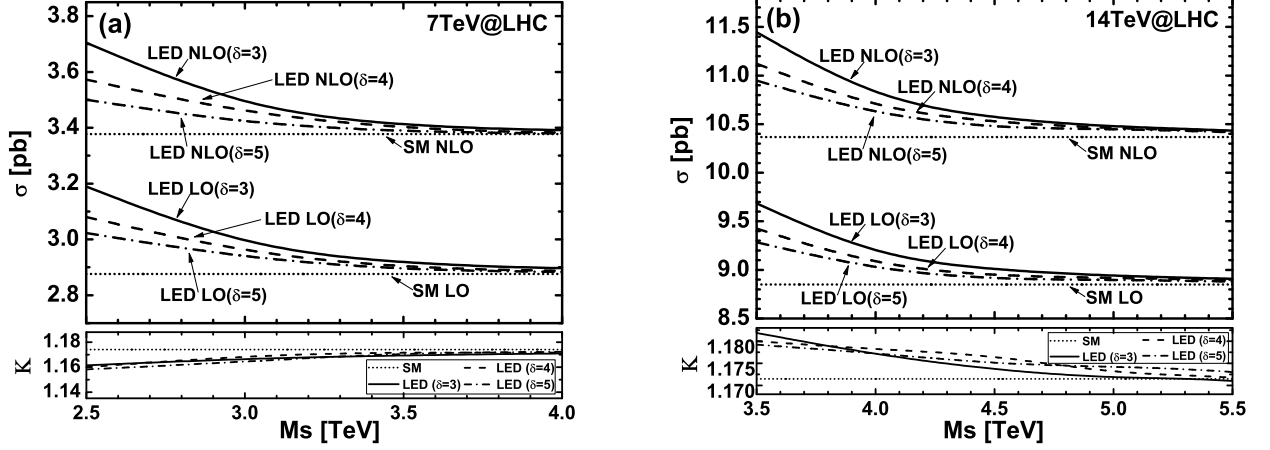


Figure 10: The LO and NLO QCD corrected cross sections and the corresponding  $K$ -factors for the process  $pp \rightarrow W^+W^- + X$  in the LED model as functions of  $M_S$  with  $\mu = m_W$  and  $\delta = 3, 4, 5$ . (a) At the  $\sqrt{s} = 7 \text{ TeV}$  LHC. (b) At the  $\sqrt{s} = 14 \text{ TeV}$  LHC.

dimensions and obtained by taking the input parameters and the event selection constraints mentioned above. As we expected, the LO and NLO QCD corrected differential cross sections of the  $W$ -pair invariant mass become less with the increment of  $M_{WW}$ .

It is clear that if the deviation of the cross section from the SM prediction is large enough, the LED effect including the NLO QCD corrections can be found. We assume that the LED effect can and cannot be observed, only if

$$\Delta\sigma_{NLO} = |\sigma_{NLO}^{LED} - \sigma_{NLO}^{SM}| \geq \frac{5\sqrt{\mathcal{L}\sigma_{NLO}^{LED}}}{\mathcal{L}} \equiv 5\sigma \quad (5.1)$$

and

$$\Delta\sigma_{NLO} = |\sigma_{NLO}^{LED} - \sigma_{NLO}^{SM}| \leq \frac{3\sqrt{\mathcal{L}\sigma_{NLO}^{LED}}}{\mathcal{L}} \equiv 3\sigma, \quad (5.2)$$

respectively. In Figs.12(a,b), we present the discovery and exclusion regions in the luminosity-fundamental scale space ( $\mathcal{L} - M_S$ ) for the  $pp \rightarrow W^+W^- + X$  process with  $\delta = 3$ . Figure.12(a) is for the  $\sqrt{s} = 7 \text{ TeV}$  LHC and Fig.12(b) for the  $\sqrt{s} = 14 \text{ TeV}$  LHC, where the LED effect can and cannot be observed in the dark and gray- region, separately. We list some typical data which are read out from Figs.12(a,b) in Table 3. There the discovery and exclusion fundamental scale  $M_S$  values at the early and future LHC are presented. It shows that by using the  $W$ -boson

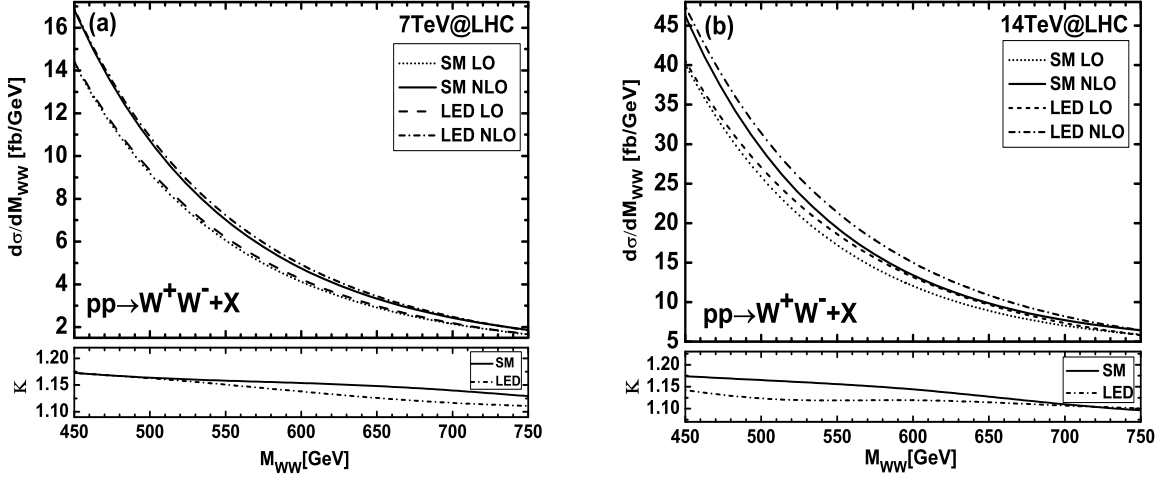


Figure 11: The LO and NLO QCD corrected distributions of the  $W$ -pair invariant mass ( $d\sigma_{LO}/dM_{WW}$ ,  $d\sigma_{NLO}/dM_{WW}$ ) and the corresponding  $K$ -factors for  $pp \rightarrow W^+W^- + X$  with  $M_S = 3.5 \text{ TeV}$ ,  $\mu = m_W$  and  $\delta = 3$  in the SM and LED model. (a) At the  $\sqrt{s} = 7 \text{ TeV}$  LHC. (b) At the  $\sqrt{s} = 14 \text{ TeV}$  LHC.

pair production events we could set an exclusion limit on the cutoff scale  $M_S$  to be  $1.80 \text{ TeV}$  at the 95% confidence level at the  $\sqrt{s} = 7 \text{ TeV}$  LHC with an integrated luminosity of  $36 \text{ (pb)}^{-1}$ . This is in the  $M_S$  lower limit range of  $1.6 \sim 2.3 \text{ TeV}$  obtained experimentally by the CMS using the diphoton final state data samples [7].

Luminosity( $\mathcal{L}$ ) ( $\mathcal{L}$ )	$\sqrt{s} = 7 \text{ TeV}$		$\sqrt{s} = 14 \text{ TeV}$	
	$M_S[\text{TeV}](3\sigma)$	$M_S[\text{TeV}](5\sigma)$	$M_S[\text{TeV}](3\sigma)$	$M_S[\text{TeV}](5\sigma)$
$100 \text{ fb}^{-1}$	3.83	3.50	5.69	5.46
$200 \text{ fb}^{-1}$	3.98	3.74	5.79	5.62
$300 \text{ fb}^{-1}$	4.17	3.85	5.83	5.70
$36 \text{ pb}^{-1}$	1.80	1.68	2.03	1.89

Table 3: The discovery ( $\Delta\sigma_{tot} \geq 5\sigma$ ) and exclusion ( $\Delta\sigma_{tot} \leq 3\sigma$ ) LED model fundamental scale ( $M_S$ ) values for the  $pp \rightarrow W^+W^- + X$  process at the early ( $\sqrt{s} = 7 \text{ TeV}$ ) and future ( $\sqrt{s} = 14 \text{ TeV}$ ) LHC.

Now we consider the subsequential leptonic (electron, muon) decay of one of the two  $W$ -bosons. In collecting the  $pp \rightarrow W^+W^- \rightarrow W^\pm l^\mp \nu_l^{(-)} + X$  ( $\ell = e, \mu$ ) events we do not distinguish the leptonic charge. We fix the branching fraction for  $W$ -boson decay ( $W^\mp \rightarrow \ell^\mp \nu^{(-)}$ ,  $\ell = e, \mu$ ) as 21.32% [17],  $\mathcal{L} = 300 \text{ fb}^{-1}$ , and take the number of the extra dimensions  $\delta = 3$ , the constraints

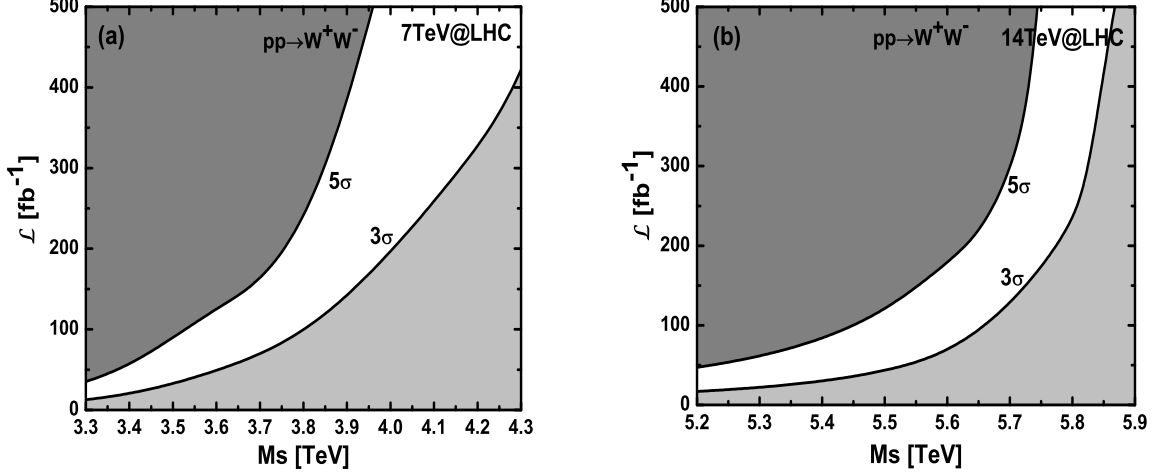


Figure 12: The LED effect discovery area (dark) and the exclusion area (gray) in the  $\mathcal{L} - M_S$  space for the  $pp \rightarrow W^+W^- + X$  process. (a) At the  $\sqrt{s} = 7 \text{ TeV}$  LHC. (b) At the  $\sqrt{s} = 14 \text{ TeV}$  LHC.

of  $M_{WW} > 400 \text{ GeV}$ ,  $p_T^l > p_{T,l}^{cut} = 100 \text{ GeV}$ , and the jet event selection criterion as declared above. We show the discovery and exclusion regions in the  $\mathcal{L} - M_S$  space for the processes  $pp \rightarrow W^+W^- \rightarrow W^\pm l^\mp \bar{\nu}_l^{(-)} + X$  ( $\ell = e, \mu$ ) in Figs.13(a) and (b) for the  $\sqrt{s} = 7 \text{ TeV}$  and  $\sqrt{s} = 14 \text{ TeV}$  LHC, respectively, The dark and gray- regions represent the parameter space where the LED effect can and cannot be observed separately. Some representative data for the discovery and exclusive fundamental scale  $M_S$  values at the early ( $\sqrt{s} = 7 \text{ TeV}$ ) and future ( $\sqrt{s} = 14 \text{ TeV}$ ) LHC read out from Figs.13(a,b) are presented in Table 4. We can see from the table that by using  $pp \rightarrow W^+W^- \rightarrow W^\pm l^\mp \bar{\nu}_l^{(-)} + X$  ( $\ell = e, \mu$ ) processes with the constraints of  $M_{WW} > 400 \text{ GeV}$ ,  $p_T^l > p_{T,l}^{cut} = 100 \text{ GeV}$ , and our chosen jet event selection criterion, we could get exclusion lower limit on  $M_S$  as  $2.19 \text{ TeV}$  at the 95% confidence level at the  $\sqrt{s} = 7 \text{ TeV}$  LHC with an integrated luminosity of  $36 \text{ (pb)}^{-1}$ , which is larger than that obtained by analyzing the  $W$ -pair production events as described above.

We depict the LED discovery and exclusion regions in the  $M_S - p_{T,l}^{cut}$  space for the processes  $pp \rightarrow W^+W^- \rightarrow W^\pm l^\mp \bar{\nu}_l^{(-)} + X$  ( $\ell = e, \mu$ ) in Figs.14(a) and (b) with  $\delta = 3$ ,  $\mathcal{L} = 300 \text{ fb}^{-1}$ ,  $M_{WW} > 400 \text{ GeV}$ , and the branching fraction for  $W$ -boson decays ( $W^\mp \rightarrow \ell^\mp \bar{\nu}_l^{(-)}$ ,  $\ell = e, \mu$ ) as 21.32%, where Fig.14(a) and Fig.14(b) are for the  $\sqrt{s} = 7 \text{ TeV}$  and  $\sqrt{s} = 14 \text{ TeV}$  LHC

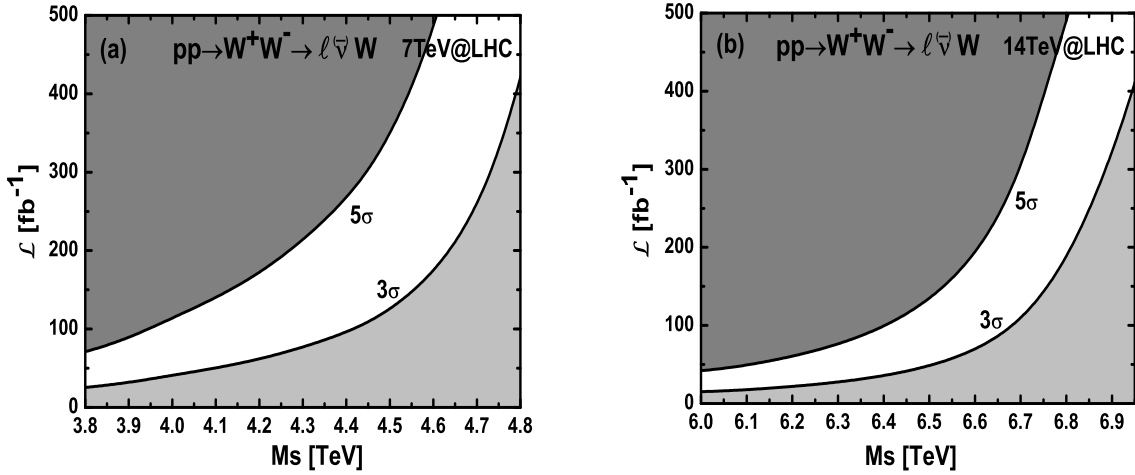


Figure 13: The LED effect discovery area (dark) and exclusion area (gray) in the  $\mathcal{L} - M_S$  space for the  $pp \rightarrow W^+W^- \rightarrow W^\pm l^\mp \bar{\nu}_l^{(-)} + X$  ( $\ell = e, \mu$ ) processes with the constraints of  $M_{WW} > 400 \text{ GeV}$ ,  $p_T^l > p_{T,l}^{cut} = 100 \text{ GeV}$ , and the jet event selection criterion declared above. (a) at the  $\sqrt{s} = 7 \text{ TeV}$  LHC. (b) at the  $\sqrt{s} = 14 \text{ TeV}$  LHC.

Luminosity( $\mathcal{L}$ ) ( $\mathcal{L}$ )	$\sqrt{s} = 7 \text{ TeV}$		$\sqrt{s} = 14 \text{ TeV}$	
	$M_S[\text{TeV}](3\sigma)$	$M_S[\text{TeV}](5\sigma)$	$M_S[\text{TeV}](3\sigma)$	$M_S[\text{TeV}](5\sigma)$
100 $fb^{-1}$	4.42	3.95	6.69	6.41
200 $fb^{-1}$	4.65	4.29	6.82	6.62
300 $fb^{-1}$	4.74	4.45	6.87	6.71
36 $pb^{-1}$	2.19	1.96	2.98	2.80

Table 4: The discovery ( $\Delta\sigma_{tot} \geq 5\sigma$ ) and exclusion ( $\Delta\sigma_{tot} \leq 3\sigma$ ) fundamental scale ( $M_S$ ) values for the  $pp \rightarrow W^+W^- \rightarrow W^\pm l^\mp \bar{\nu}_l^{(-)} + X$  ( $\ell = e, \mu$ ) processes in the  $\mathcal{L} - M_S$  space for the  $pp \rightarrow W^+W^- \rightarrow W^\pm l^\mp \bar{\nu}_l^{(-)} + X$  ( $\ell = e, \mu$ ) processes with the constraints of  $M_{WW} > 400 \text{ GeV}$  and  $p_T^l > p_{T,l}^{cut} = 100 \text{ GeV}$ : at the  $\sqrt{s} = 7 \text{ TeV}$  LHC and at the  $\sqrt{s} = 14 \text{ TeV}$  LHC.

respectively. The dark and gray- regions represent the parameter regions where the LED effect can and cannot be observed, separately, with the constraints of  $p_{T,l} > p_{T,l}^{cut}$  and the  $W$ -pair invariant mass  $M_{WW} > 400 \text{ GeV}$ . Some representative data are listed in Table 5 for the discovery and exclusion fundamental scale  $M_S$  values with different  $p_{T,l}^{cut}$  values at the  $\sqrt{s} = 7 \text{ TeV}$  and  $\sqrt{s} = 14 \text{ TeV}$  LHC as shown in Figs.14(a,b). We can see that in the case where we fix the integral luminosity (e.g.  $\mathcal{L} = 300 \text{ fb}^{-1}$ ), we could improve slightly the low limit on  $M_S$  if we adopt a larger lower cut on lepton transverse momentum ( $p_{T,l}^{cut}$ ).

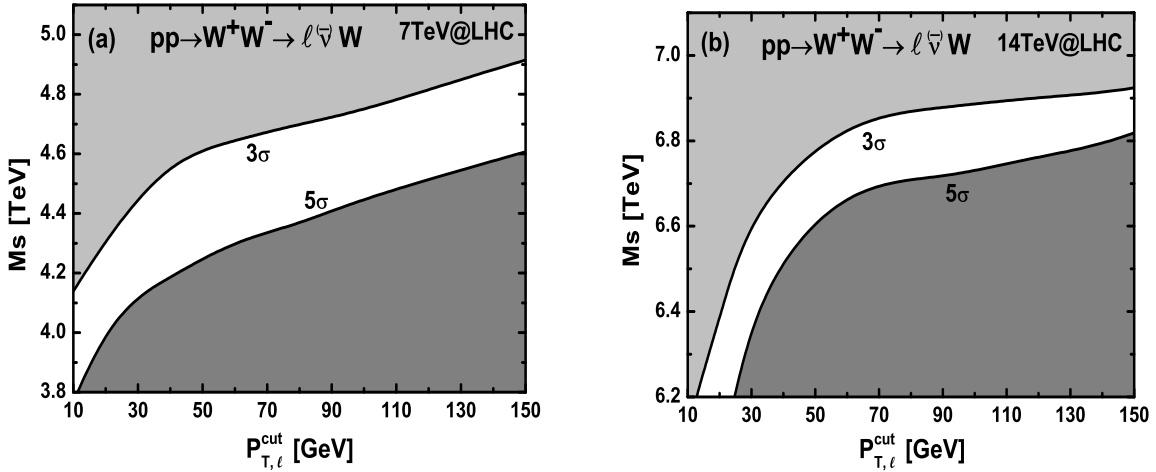


Figure 14: The LED effect discovery area (dark) and exclusion area (gray) in the  $M_S - p_{T,l}^{cut}$  space for the  $pp \rightarrow W^+W^- \rightarrow W^\pm l^\mp \bar{\nu}_l + X$  ( $l = e, \mu$ ) processes with  $\delta = 3$  and  $\mathcal{L} = 300 \text{ fb}^{-1}$ . (a) At the  $\sqrt{s} = 7 \text{ TeV}$  LHC. (b) At the  $\sqrt{s} = 14 \text{ TeV}$  LHC.

$p_T^l$ cut value ( $p_{T,l}^{cut}$ )	7 TeV		14 TeV	
	$M_S[\text{TeV}](3\sigma)$	$M_S[\text{TeV}](5\sigma)$	$M_S[\text{TeV}](3\sigma)$	$M_S[\text{TeV}](5\sigma)$
50 GeV	4.61	4.24	6.67	6.60
100 GeV	4.74	4.45	6.87	6.71
150 GeV	4.92	4.61	6.92	6.80

Table 5: The discovery ( $\Delta\sigma_{tot} \geq 5\sigma$ ) and exclusion ( $\Delta\sigma_{tot} \leq 3\sigma$ ) LED model fundamental scale ( $M_S$ ) values in the  $M_S - p_{T,l}^{cut}$  space for the  $pp \rightarrow W^+W^- \rightarrow W^\pm l^\mp \bar{\nu}_l + X$  ( $l = e, \mu$ ) processes with the constraints of  $M_{WW} > 400 \text{ GeV}$  and  $p_T^l > p_{T,l}^{cut}$ . (a) at the  $\sqrt{s} = 7 \text{ TeV}$  LHC. (b) at the  $\sqrt{s} = 14 \text{ TeV}$  LHC.

## VI. Summary

We calculate the NLO QCD corrections to the  $pp \rightarrow W^+W^- \rightarrow W^\pm l^\mp \bar{\nu} + X$  process in the SM and LED model at the LHC. We investigate the integrated cross sections, the distributions of some kinematic variables and how they are affected by radiative corrections. The calculations are compared with previous works, and finally the reliable numerical results are obtained. We find that the NLO QCD corrected results do not show remarkable reduction of the scale uncertainties of the LO cross sections in both the SM and LED model, because the uncertainty of the LO cross section is underestimated. The scale-dependent  $K$ -factor is found to be the value from 1.18 (1.53) to 1.19 (1.11) when  $\mu$  goes from  $0.5\mu_0$  to  $2\mu_0$  at the  $\sqrt{s} = 7 \text{ TeV}$  ( $\sqrt{s} = 14 \text{ TeV}$ ) LHC, with the constraints of  $M_{WW} > 400 \text{ GeV}$  and our jet event selection criterion. The  $5\sigma$  discovery and  $3\sigma$  exclusion ranges for the LED parameters  $M_S$  are also obtained in the NLO QCD. The inclusion of the effects of the virtual KK graviton turns out to enhance the differential distributions of kinematical observables generally. We conclude that the NLO QCD correction to the  $W$ -pair production make it possible to precisely test the  $TeV$  quantum gravity in the LED scenario at the LHC.

**Acknowledgments:** This work was supported in part by the National Natural Science Foundation of China (No.10875112, No.11075150, No.11005101), and the Specialized Research Fund for the Doctoral Program of Higher Education(No.20093402110030).

## References

- [1] Nima Arkani-Hamed, Savas Dimopoulos, G.R. Dvali, Phys. Lett. **B 429**,263(1998), arXiv:hep-ph/9803315; Phys. Rev. **D59** 086004(1999); I. Antoniadis, N. Arkani-Hamed, S. Dimopoulos, G. Dvali, Phys. Lett. **B 436**,257(1998)
- [2] Tao Han, Joseph D. Lykken, Ren-Jie Zhang, Phys. Rev. **D59**,105006(1999), arXiv:hep-ph/9811350.
- [3] Gian F. Giudice, Riccardo Rattazzi, James D. Wells, Nucl. Phys. **B544**,3(1999),

- arXiv:hep-ph/9811291.
- [4] Prakash Mathews, V. Ravindran, K. Sridhar, W.L. van Neerven, Nucl. Phys. **B713**,333(2005), arXiv:hep-ph/0411018.
- [5] Prakash Mathews, V. Ravindran, K. Sridhar, JHEP **0408**,048,2004, arXiv:hep-ph/0405292.
- [6] N. Agarwal, V. Ravindran, V.K. Tiwari, A. Tripathi, Nucl. Phys. **B830**, 248(2010). e-Print: arXiv:0909.2651. M.C. Kumar, P. Mathews, V. Ravindran, An. Tripathi, Phys. Lett. **B672**,45(2009). e-Print: arXiv:0811.1670
- [7] S. Chatrchyan et al. (CMS Collaboration), J. High Energy Phys. 05(2011)085
- [8] R. Franceschini, G. Francesco Giudice, P. P. Giardino, P. Lodone, A. Strumia, JHEP, 1105 (2011) 092, arXiv:1101.4919.
- [9] N. Agarwal, V. Ravindran, V.K. Tiwari, A. Tripathi, Phys. Rev. **D82**,036001(2010), arXiv:1003.5450.
- [10] Thomas Hahn, Comput. Phys. Commun. **140**,418(2001). arXiv:hep-ph/0012260
- [11] T. Hahn, M. Perez-Victoria, Comput. Phys. Commun. **118**,153(1999). arXiv:hep-ph/9807565
- [12] B.W. Harris, J.F. Owens, Phys. Rev. **D65**,094032(2002). arXiv:hep-ph/0102128
- [13] S.Dittmaier, S.Kallweit, P. Uwer, Nucl. Phys.**B826**,18(2010). arXiv:0908.4124
- [14] John C. Collins, Davison E. Soper, George F. Sterman, Nucl. Phys.**B261**,104(1985).
- [15] T. Kinoshita, J. Math. Phys.3:650-677,1962; T.D. Lee, M. Nauenberg, Phys. Rev. 133, B1549(1964).
- [16] J. M. Campbell, R. K. Ellis, Phys. Rev. **D60**,113006(1999), arXiv:hep-ph/9905386.
- [17] K. Nakamura et al. (Particle Data Group), J. Phys.**G37**,075021(2010).



- [18] J. Pumplin, D.R. Stump, J. Huston, H.L. Lai, Pavel M. Nadolsky, W.K. Tung, *JHEP* **0207**,012(2002), arXiv:hep-ph/0201195.
- [19] Daniel Stump, Joey Huston, Jon Pumplin, Wu-Ki Tung, H.L. Lai, Steve Kuhlmann, J.F. Owens, *JHEP* **0310**,046(2003), arXiv:hep-ph/0303013.